Dinuclear Rhodium(I) and Iridium(I) Dicarboxytriazolate Complexes and Their Oxidation Products. Crystal Structures of $[NBu_4][Rh_2(Dcbt)(CO)_4]\cdot 0.4CH_2Cl_2$ and $[NBu_4][Rh_2(Dcbt)(CO)_2(PPh_3)_2]$

G. Net, J. C. Bayón,* and P. Esteban

Departament de Química, Universitat Autònoma de Barcelona, Bellaterra, 08193 Barcelona, Spain

P. G. Rasmussen

Department of Chemistry, The University of Michigan, Ann Arbor, Michigan 48109

A. Alvarez-Larena and J. F. Piniella

Departament de Geologia (Unitat de Cristal.lografia), Universitat Autònoma de Barcelona, Bellaterra, 08193 Barcelona, Spain

Received February 11, 1993•

4,5-Dicarboxytriazole (H_3Dcbt) has been found to be a dinucleating ligand with behavior similar to that of other dicarboxyazolates previously reported. A new family of anionic complexes of this ligand with Rh(I) and Ir(I) using cyclooctadiene, CO, and PPh_3 as ancillary ligands have been prepared. The salt $[NBu_4][Rh_2(Dcbt)(CO)_4]\cdot 0.4CH_2Cl_2$ crystallizes in the monoclinic space group $P2_1/c$ with $a = 14.210(4)$ Å, $b = 16.161(4)$ Å, $c = 15.296(4)$ Å, and $\beta = 114.42(2)°$ and with four anions and four cations per unit cell. The final R value was 0.036. The planar anions $[Rh_2(Dcbt)(CO)_4]^-$ form dimers separated by cations. The short distance between the rhodium atoms in the dimer is associated with metal–metal interactions. The product $[NBu_4][Rh_2(Dcbt)(CO)_2(PPh_3)_2]$ crystallizes in the triclinic space group $P\bar{1}$ with $a = 17.714(8)$ Å, $b = 12.969(8)$ Å, $c = 13.406(8)$ Å, $\alpha = 108.15(4)°$, $\beta = 101.38(4)°$, and $\gamma = 95.95(4)°$ and with two anions and two cations per unit cell. The final R value was 0.053. The triphenylphosphine is situated *trans* to N due to the larger *trans* effect of the ring N atom. The electrochemical oxidation of $[NR_4][Ir_2(Dcbt)(CO)_4]$ (R = Pr, Bu) yielded the partially oxidized conductive materials $[NR_4]_{0.5}[Ir_2(Dcbt)(CO)_4]$. The stoichiometry based on elemental analyses was corroborated by X-ray photoelectron spectroscopy (XPS). This technique showed also that the oxidation is metal centered. An EXAFS study indicated that the coordination sphere of the iridium is preserved upon oxidation. The pressed pellet conductivities of these partially oxidized salts are in the range 10^{-4}–10^{-5} Ω^{-1} cm^{-1}.

Introduction

Electrical conductivity and mixed-valence charge transfer are solid-state properties which have been of great interest in recent years, especially since the reports of the structure of Krogmann's salt.[1] A number of additional examples have been reported, in which the metal–metal interactions along the stacking axis dominate the properties. Among them, the families of bis(oxalato)platinates[2] and chlorocarbonyliridates[3] are the most typical. The factors which control the stacking and metal–metal interactions are in delicate balance and are influenced by interstack interactions, counterion packing,[4] and Peierls distortions.[5] We have been particularly interested in knowing how the use of dinuclear metal complexes would influence the stacking and properties of these type of materials.

Our strategy was to design a number of planar complexes of rhodium and iridium with a central dicarboxyazolate ligand. We wished to know what kinds of stacking motifs could be observed and what the effect an aromatic ligand, coupling the metal ions in a second dimension, might have on the properties. Previously we reported on the following heteroaromatic dicarboxyazolates: the trianions of 4,5-imidazoledicarboxylic acid (H_3Dcbi),[6] 2-methyl-4,5-imidazoledicarboxylic acid (H_3MDcbi),[6–8] and 3,5-pyrazoledicarboxylic acid (H_3Dcbp)[9] and the dianions of 2,3-pyrazinedicarboxylic acid (H_2cDcp) and 2,5-pyrazinedicarboxylic acid (H_2tDcp).[10] In these studies we found that the planar anionic complexes $[Ir_2(A)(CO)_4]^-$ (A = Dcbi, MDcbi, Dcbp) form, upon electrochemical oxidation, conductive solids of composition $[NR_4]_{0.5}[Ir_2(A)(CO)_4]$ (R = Pr, Bu) ($\sigma = 10^{-5}$–10^{-4} Ω^{-1} cm^{-1} for pressed pellets). Conversely, neither the anionic $[Rh_2(A)(CO)_4]^-$ (A = Dcbi, MDcbi, Dcbp) nor the neutral $[M_2(A)(CO)_4]$ (M = Rh, Ir; A = cDcp, tDcp)[10] formed conductive materials. The oxidation of the anionic complexes of rhodium yielded the neutral nonconductive products $[Rh_2(A)(CO)_4]$ (A = Dcbi, MDcbi,

• Abstract published in *Advance ACS Abstracts*, August 15, 1993.

(1) (a) Krogmann, K. *Angew. Chem., Int. Ed. Engl.* **1969**, *8*, 35. (b) *Extended Linear Chain Compounds*; Miller, J. S., Ed.; Plenum: New York, 1981; Vol. 1, p 90.
(2) (a) Underhill, A. E.; Watkins, D. M. *Chem. Soc. Rev.* **1980**, *9*, 429. (b) *Extended Linear Chain Compounds*; Miller, J. S., Ed.; Plenum: New York, 1981; Vol. 1, p 119.
(3) (a) Gingsberg, A. P.; Koepe, J. W.; Hauser, J. J.; West, K. W.; Di Salvo, F. J.; Sprinkle, C. R.; Cohen, R. L. *Inorg. Chem.* **1976**, *15*, 514. (b) Buravov, L. N.; Stepanova, R. N.; Khidekel, M. L.; Shchegolev, I. F. *Dokl. Akad. Nauk SSSR* **1972**, *203*, 819.
(4) Rasmussen, P. G.; Kolowich, J. B.; Bayón, J. C. *J. Am. Chem. Soc.* **1988**, *110*, 7042.
(5) Peierls, R. E. *Quantum Theory of Solids*; Oxford University Press: London, 1955; p 108.
(6) Bayón, J. C.; Net, G.; Rasmussen, P. G.; Kolowich, J. B. *J. Chem. Soc., Dalton Trans.* **1987**, 3003.
(7) Anderson, J. E.; Gregory, T. P.; Net, G.; Bayón, J. C. *J. Chem. Soc., Dalton Trans.* **1992**, 487.
(8) Net, G.; Bayón, J. C.; Butler, W. M.; Rasmussen, P. G. *J. Chem. Soc., Chem. Commun.* **1989**, 1022.
(9) Bayón, J. C.; Net, G.; Esteban, P.; Rasmussen, P. G.; Bergstrom, D. F. *Inorg. Chem.* **1991**, *30*, 4771.
(10) Bayón, J. C.; Net, G.; Real, J.; Rasmussen, P. G. *J. Organomet. Chem.* **1990**, *385*, 409.

0020-1669/93/1332-5313$04.00/0

Dcbp). The neutral compounds with pyrazines could not be oxidized because of their insolubility.

In order to expand this group of dinuclear conducting materials and to evaluate the role of the anionic character of the metal complex, we have investigated a new family of products containing the trianion of 4,5-triazoledicarboxylic acid (H_3Dcbt). Since H_3Dcbt is more acidic than the ligands previously investigated, the new family could also allow the study of the ligand acidity influence on the synthesis and properties of conducting materials. We also wished to confirm that the behaviors of rhodium and iridium are quite distinct in this chemistry, which had been suggested in our earlier results.

Experimental Section

All reactions were performed under nitrogen by using standard Schlenk techniques. Solvents were purified and dried by standard procedures. $[M_2(\mu\text{-Cl})_2(\text{cod})_2]$,[11,12] $[M_2(\mu\text{-OMe})_2(\text{cod})_2]$[13] (M = Rh, Ir; cod = 1,5-cyclooctadiene), 4,5-dicyano-1,2,3-triazole,[14] 1,2,3-triazole-4,5-dicarboxylic acid,[14] and $[TTF]_3[BF_4]_2$ (TTF^+ = tetrathiafulvalenium)[15] were prepared by reported procedures.

Physical Measurements. Elemental analyses of C, H, and N were performed on a Perkin-Elmer 240-C. Iridium was analyzed gravimetrically after heating the samples at 900 °C. Infrared spectra (4000–400 cm^{-1}) were recorded on a Perkin-Elmer Model 1710 infrared Fourier transform spectrometer. Fourier transform ^1H and $^{13}C\{^1H\}$ NMR spectra were recorded on a Bruker AM400 instrument. Chemical shifts for these spectra are reported relative to tetramethylsilane. A six-channel constant-current source manufactured by Sambrook Engineering (Wales, U.K.) was used for the electrosyntheses. Specially designed two- or three-compartment anaerobic cells were used. Platinum electrodes were used, and they were electrolytically cleaned before each synthesis. XPS spectra were recorded on a Vacuum Generators (VG) ESCA III spectrometer using Al Kα radiation (1486.6 eV) as a source of photons. This apparatus was equipped with a Digital PDP computer system for data acquisition. The carbon 1s photoelectron line (285.0 eV) was used for the calibration.[16] The X-ray absorption spectra were recorded on the EXAFS I spectrometer at LURE-DCI (Paris) using a silicon(331) monochromator, the ring running at 1.85 GeV and 280 mA. A local program was used to extract the structural information from EXAFS data.[17] Data were analyzed by using calculated amplitude and phase functions for the iridium atom[18] and for the scatters C, O, and N,[19] since no suitable models were found for the second-shell distances (Ir–O and Ir–C = *ca.* 3 Å). Amplitude and phase functions derived from metallic iridium were used to simulate the Ir–Ir contributions. Conductivity measurements were performed on pressed pellets using the van der Pauw method.[20] Silver epoxy resin was used as contacts. Keithley 175 and 610C electrometers were used to measure voltages and intensities, respectively. Constant current was generated with a Sambrook current source.

Synthesis of $[NR_4][M_2(\text{Dcbt})(\text{cod})_2]$ (R = Bu, Pr, Me; M = Rh, Ir). Method A. $[Bu_4N]OH$ (12 mL) 0.1 M in toluene/methanol (Merck), $[Me_4N]OH$ (12 mL) 0.1 M in 2-propanol/methanol (Merck), or 0.8 mL of $[Pr_4N]OH$ 20% in water (Merck) was added dropwise to a suspension of 0.4 mmol of $[M_2(\mu\text{-Cl})_2(\text{cod})_2]$ (M = Rh, Ir) and 0.4 mmol of 4,5-dicarboxytriazole in 10 mL of acetonitrile. After 10 min of stirring, the solvents were removed and the yellow residue was dissolved in 10 mL of acetonitrile and 0.5 mL of methanol (10 mL of 2-propanol in the case of $[NBu_4][Rh_2(\text{Dcbt})(\text{cod})_2]$). Yellow crystals were obtained by slow evaporation (yield ~80%).

Method B (Only for Iridium Compounds). A 4-mL portion of $[Bu_4N]OH$ 0.1 M in toluene/methanol (Merck) or $[Me_4N]OH$ 0.1 M in 2-propanol/methanol (Merck) or 0.27 mL of $[Pr_4N]OH$ 20% in water (Merck) was added dropwise to a suspension of 0.4 mmol of $[Ir_2(\mu\text{-OMe})_2(\text{cod})_2]$ and 0.4 mmol of 4,5-dicarboxytriazole in 10 mL of acetonitrile. After the mixture was stirred for 1 h, the solvents were evaporated in vacuo. Redissolution of the residue in a minimum of methylene chloride followed by slow addition of hexane to form an upper layer afforded small yellow crystals of the product. Yield was nearly quantitative.

Anal. Calcd for $[NBu_4][Rh_2(\text{Dcbt})(\text{cod})_2]$, $C_{36}H_{60}N_4O_4Rh_2$: C, 52.8; H, 7.39; N, 6.84. Found: C, 52.3; H, 7.45; N, 6.81. IR (KBr): 1667 cm^{-1} (OCO asym). IR (CH_2Cl_2): 1654 cm^{-1} (OCO asym). NMR ($CDCl_3$), δ, ppm: ^1H, 4.28 (s, b, CH of cod), 2.34, 1.77 (m, CH_2 of cod); $^{13}C\{^1H\}$, 167.4 (CO_2), 139.9 (C4, C5), 82.6 (d, CH of cod *trans* N, J(Rh–C) = 12.0 Hz), 72.3 (d, CH of cod *trans* O, J(Rh–C) = 13.8 Hz), 30.1, 29.2 (CH_2 of cod).

Anal. Calcd for $[NMe_4][Rh_2(\text{Dcbt})(\text{cod})_2]\cdot H_2O$, $C_{24}H_{38}N_4O_5Rh_2$: C, 43.1; H, 5.73; N, 8.38. Found: C, 42.9; H, 5.70; N, 8.41. IR (KBr): 1630, 1682 cm^{-1} (OCO asym).

Anal. Calcd for $[NBu_4][Ir_2(\text{Dcbt})(\text{cod})_2]$, $C_{36}H_{60}N_4O_4Ir_2$: C, 43.4; H, 6.06; N, 5.62. Found: C, 43.3; H, 6.00; N, 5.88. IR (KBr): 1685 cm^{-1} (OCO asym). IR (CH_2Cl_2): 1680 cm^{-1} (OCO asym). NMR ($CDCl_3$), δ, ppm: ^1H, 4.22 (s, b, CH of cod), 2.21, (m, CH_2 of cod); $^{13}C\{^1H\}$, 169.3 (CO_2), 140.2 (C4, C5), 68.7 (CH of cod *trans* N), 56.0 (CH of cod *trans* O), 31.8, 31.0 (CH_2 of cod).

Anal. Calcd for $[NPr_4][Ir_2(\text{Dcbt})(\text{cod})_2]$, $C_{32}H_{52}N_4O_4Ir_2$: C, 40.8; H, 5.57; N, 5.95. Found: C, 40.3; H, 5.62; N, 5.93. IR (KBr): 1663 cm^{-1} (OCO asym).

Anal. Calcd for $[NMe_4][Ir_2(\text{Dcbt})(\text{cod})_2]$, $C_{24}H_{36}N_4O_4Ir_2$: C, 34.8; H, 4.38; N, 6.76. Found: C, 35.1; H, 4.40; N, 6.72. IR (KBr): 1694 cm^{-1} (OCO asym).

Synthesis of $[NR_4][M_2(\text{Dcbt})(\text{CO})_4]$ (R = Bu, Pr; M = Rh, Ir). Carbon monoxide was slowly bubbled through solutions of $[NR_4][M_2(\text{Dcbt})(\text{cod})_2]$ salts in methylene chloride. Hexane was carefully added to the darkened solution to form a second layer, after which crystals slowly formed (dark yellow for Bu and Rh, dichroic golden and green for Pr and Ir, and red for Bu and Ir). Yields were nearly quantitative.

Anal. Calcd for $[NBu_4][Rh_2(\text{Dcbt})(\text{CO})_4]$, $C_{24}H_{36}N_4O_8Rh_2$: C, 40.4, H, 5.08; N, 7.84. Found: C, 40.2; H, 5.08; N, 7.79. IR (KBr): 2086, 2077, 2018 cm^{-1} (CO), 1682, 1671 cm^{-1} (OCO asym). IR (CH_2Cl_2): 2084, 2017 cm^{-1} (CO), 1683 cm^{-1} (OCO asym).

Anal. Calcd for $[NBu_4][Ir_2(\text{Dcbt})(\text{CO})_4]$, $C_{24}H_{36}N_4O_8Ir_2$: C, 32.3; H, 4.06; N, 6.27. Found: C, 32.1; H, 3.96; N, 6.27. IR (KBr): 2054, 2004, 1983 cm^{-1} (CO), 1693 cm^{-1} (OCO asym). IR (CH_2Cl_2): 2072, 2001 cm^{-1} (CO), 1699 cm^{-1} (OCO asym).

Anal. Calcd for $[NPr_4][Ir_2(\text{Dcbt})(\text{CO})_4]$, $C_{20}H_{28}N_4O_8Ir_2$: C, 28.7; H, 3.37; N, 6.69. Found: C, 29.0; H, 3.49; N, 6.66. IR (KBr): 2087, 2027 cm^{-1} (CO), 1658, 1652 cm^{-1} (OCO asym).

Synthesis of $[NMe_4][M_2(\text{Dcbt})(\text{CO})_4]$ (M = Rh, Ir). Carbon monoxide was slowly bubbled through solutions of $[NMe_4][M_2(\text{Dcbt})(\text{cod})_2]$ salts in CH_3CN (M = Rh) or DMSO (M = Ir). A dark compound precipitated (fine needles in the case of M = Rh). Yield was approximately 70%.

Anal. Calcd for $[NMe_4][Rh_2(\text{Dcbt})(\text{CO})_4]\cdot H_2O$ (dichroic copper and violet shiny needles), $C_{12}H_{14}N_4O_9Rh_2$: C, 25.6; H, 2.50; N, 9.93. Found: C, 25.9; H, 2.50; N, 9.91. IR (KBr): 2087, 2072, 2019, 2006 cm^{-1} (CO), 1680 cm^{-1} (OCO asym).

Anal. Calcd for $[NMe_4][Ir_2(\text{Dcbt})(\text{CO})_4]\cdot 3H_2O$ (dark brown amorphous product), $C_{12}H_{20}N_4O_{12}Ir_2$: C, 18.5; H, 2.33; N, 7.19. Found: C, 18.1; H, 2.16; N, 6.98. IR (KBr): 2089, 2011 (CO), 1663 (OCO asym).

Synthesis of $[TTF][Rh_2(\text{Dcbt})(\text{CO})_4]\cdot 0.5CH_3CN\cdot H_2O$. Method A. A solution of $[TTF]_3[BF_4]_2$ (0.1 mmol) in acetonitrile (10 mL) was added slowly to a solution of $[NBu_4N][Rh_2(\text{Dcbt})(\text{CO})_4]$ (0.1 mmol) in the same solvent (5 mL). A dichroic product, green and dark red, formed during the addition. The reaction mixture was stirred for 0.5 h, and finally the solid was filtered off, rinsed with acetonitrile, and dried under vacuum.

Method B. A solution of $[Bu_4N][Rh_2(\text{Dcbt})(\text{CO})_4]$ (0.1 mmol) and tetrathiafulvalene (TTF) (0.1 mmol) in 10 mL of acetonitrile was placed in the anode side of an electrochemical cell and oxidized at constant current (1 μA). A solution of similar ionic strength in $[Bu_4N][BF_4]$ was placed in the cathode. The dichroic product that formed on the anode was scraped off and dried under vacuum.

Anal. Calcd for $C_{15}H_{7.5}N_{3.5}O_9S_4Rh_2$: C, 25.2; H, 1.06; N, 6.86. Found: C, 24.7; H, 1.12; N, 6.82. IR (KBr): 2087, 2070, 2029, 2017 cm^{-1} (CO), 1655 cm^{-1} (OCO asym).

Synthesis of $[p\text{-}CH_3C_6H_4N_2][Rh_2(\text{Dcbt})(\text{CO})_4]$. A solution of 0.1 mmol of $[p\text{-}CH_3C_6H_4N_2][BF_4]$ in 10 mL of acetonitrile was slowly added to a solution of 0.1 mmol of $[NBu_4][Rh_2(CO)_4\text{Dcbp}]$ in 10 mL of the same solvent. A brown product slowly precipitated from the red solution. It was filtered off and rinsed with CH_3CN. Yield was 80%.

(11) Giordano, G.; Crabtree, R. H. *Inorg. Synth.* **1979**, *19*, 218.
(12) Winkhau, G.; Singer, H. *Chem. Ber.* **1966**, *99*, 3610.
(13) Usón, R.; Oro, L. A.; Cabeza, J. A. *Inorg. Synth.* **1985**, *23*, 126.
(14) Hinkel, L. E.; Richards, G. O.; Thomas, O. *J. Chem. Soc.* **1937**, 1432.
(15) Wudl, F.; Kaplan, L. *Inorg. Synth.* **1979**, *19*, 30.
(16) Programs were generously supplied by P. Legaré from the Laboratoire de Catalyse et Chimie des Surfaces (Strasbourg, France).
(17) PASCAL program written by P. Esteban.
(18) Teo, B. K.; Lee, P. A. *J. Am. Chem. Soc.* **1979**, *101*, 2815.
(19) McKale, A. G.; Veal, B. W.; Paulikas, A. P.; Chan, S. K. *J. Am. Chem. Soc.* **1988**, *110*, 3763.
(20) van der Pauw, L. J. *Philips Res. Rep.* **1958**, *13*, 1.

Table I. X-ray Data for $[NBu_4][Rh_2(Dcbt)(CO)_4]\cdot 0.4CH_2Cl_2$ (**2a**) and $[NBu_4][Rh_2(Dcbt)(CO)_2(PPh_3)_2]$ (**3a**)

	2a	**3a**
formula	$C_{24.4}H_{36.8}N_4O_8Cl_{0.8}Rh_2$	$C_{58}H_{66}N_4O_6P_2Rh_2$
mol wt	748.4	1182.9
space Group	$P2_1/c$	$P\bar{1}$
a, Å	14.210(4)	17.714(8)
b, Å	16.161(4)	12.969(8)
c, Å	15.296(4)	13.406(8)
α, deg		108.15(4)
β, deg	114.42(2)	101.38(4)
γ, deg		95.95(4)
V, Å^3	3198(2)	2824(3)
Z	4	2
d_{calc}, g cm^{-3}	1.554	1.391
μ_{calc}, cm^{-1}	11.29	7.52
radiation; λ, Å	Mo Kα; 0.710 69	Mo Kα; 0.710 69
T, °C	20	20
cryst dimens, mm	0.83 × 0.82 × 0.54	0.175 × 0.046 × 0.061
2θ limit, deg	50	45
no. of data	5164	7424
no. of data with $I > 2.5\sigma(I)$	4736	5096
no. of params	356	385
R^a	0.036	0.053
R_w^b	0.043	0.055
w	0.0028	0.00088

$^a R = \sum||F_o| - |F_d||/\sum|F_o|$. $^b R_w = [\sum w(|F_o| - |F_d|)^2/\sum w|F_o|^2]^{1/2}$.

Anal. Calcd for $C_{15}H_7N_4O_8Rh_2$: C, 30.5; H, 1.19; N, 11.9. Found: C, 30.5; H, 2.63; N, 12.6. IR (KBr): 2091, 2022 cm^{-1} (CO), 1674 cm^{-1} (OCO asym).

Synthesis of $[NBu_4][Rh_2(Dcbt)(CO)_2(PPh_3)_2]$. A solution containing equimolar amounts of $[NBu_4][Rh_2(Dcbt)(CO)_4]$ and PPh_3 in 15 mL of methylene chloride was stirred for 10 min. A yellow microcrystalline product was obtained by careful addition of a layer of hexane. Yield was nearly quantitative.

Anal. Calcd for $C_{58}H_{66}N_4O_6P_2Rh_2$: C, 58.9; H, 5.62; N, 4.74. Found: C, 57.5; H, 5.61; N, 4.70. IR (KBr): 2003, 1993, 1980 cm^{-1} (CO), 1663 cm^{-1} (OCO asym). IR (CH_2Cl_2): 1989 cm^{-1} (CO), 1654 (s), 1634 (m) cm^{-1} (OCO asym).

Synthesis of $[NMe_4][Rh_2(Dcbt)(CO)_2(PPh_3)_2]$. A solution containing equimolar amounts of $[NMe_4][Rh_2(Dcbt)(CO)_4]$ and PPh_3 in 10 mL of acetonitrile was stirred for 0.5 h. A yellow microcrystalline product formed. After slow evaporation of the solvent down to 3 mL, the product was filtered off. Yield was 80%.

Anal. Calcd for $C_{46}H_{42}N_4O_6P_2Rh_2$: C, 54.5; H, 4.17; N, 5.52. Found: C, 53.8; H, 4.01; N, 5.42. IR (KBr): 1996, 1978 cm^{-1} (CO), 1647 cm^{-1} (OCO asym).

Synthesis of $[Rh_2(Dcbt)(CO)_4]\cdot H_2O\cdot 0.5CH_3CN$. Method A. A solution of 0.1 mmol of $[C_7H_7][BF_4]$ or $NO[BF_4]$ in 10 mL of acetonitrile was slowly added to a solution of 0.1 mmol of $[NBu_4][Rh_2(Dcbt)(CO)_4]$ in 10 mL of the same solvent. A dichroic, green and dark red, product precipitated after the mixture was stirred for 0.5 h. The product was filtered off and rinsed with acetonitrile. Yield was 50%.

Method B. A solution of 0.1 mmol of $[NBu_4][Rh_2(Dcbt)(CO)_4]$ in 10 mL of acetonitrile was placed in the anode side of a two-compartment cell. An equimolar solution of $[Bu_4N][BF_4]$ was placed in the cathode. The system was electrolyzed at constant current (10 μA) until 0.9 mol of electrons/mol of product had passed (241 h). A dichroic solid slowly formed on the anode. It was scraped off, rinsed with acetonitrile, and dried under vacuum.

Anal. Calcd for $C_9H_{3.5}N_{3.5}O_9Rh_2$: C, 21.2; H, 0.70; N, 9.60. Found: C, 21.3; H, 1.10; N, 9.23. IR (KBr): 2111, 2025 cm^{-1} (CO), 1607 cm^{-1} (OCO asym).

Synthesis of $[NR_4]_{0.5}[Ir_2(Dcbt)(CO)_4]$ (R = Bu, Pr). A solution of 0.25 mmol of $[NR_4][Ir_2(Dcbt)(CO)_4]$ (R = Bu, Pr) in 25 mL of acetonitrile was placed in the anode side of a two-compartment cell and electrolyzed at constant potential (1 V). An equimolar solution of $[Bu_4N][BF_4]$ was placed in the cathode. A black product slowly formed on the anode. The reaction was stopped when 0.5 electron/molecule had passed. The solid was scraped off, rinsed with acetonitrile, and dried under vacuum.

Anal. Calcd for $[NBu_4]_{0.5}[Ir_2(Dcbt)(CO)_4]\cdot 0.5CH_3CN$, $C_{17}H_{19.5}N_4O_8Ir_2$: C, 25.8; H, 2.48; N, 7.07; Ir, 48.5. Found: C, 26.1; H, 2.61; N, 7.05; Ir, 48.6. IR (KBr): 2101, 2077, 2044, 2022, 1968 cm^{-1} (CO), 1654 cm^{-1} (OCO asym).

Table II. Selected Fractional Atomic Coordinates for $[NBu_4][Rh_2(Dcbt)(CO)_4]\cdot 0.4CH_2Cl_2$

atom	z/a	y/b	z/c	B_{eq}, Å
Rh1	0.51487(3)	0.19734(2)	0.06088(2)	6.19(1)
Rh2	0.67279(3)	−0.15921(2)	0.15521(3)	6.16(1)
N1	0.5829(3)	0.0837(2)	0.0868(2)	5.7(1)
N2	0.5621(3)	0.0119(2)	0.1150(2)	5.7(1)
N3	0.6348(3)	−0.0398(2)	0.1152(2)	5.5(1)
C4	0.7019(3)	−0.0007(3)	0.0873(3)	5.8(1)
C5	0.6679(3)	0.0789(3)	0.0687(3)	5.5(1)
C6	0.7862(3)	−0.0533(4)	0.0828(4)	6.8(2)
C7	0.7021(4)	0.1579(3)	0.0398(3)	6.6(2)
O1	0.6393(3)	0.2189(2)	0.0282(3)	8.0(1)
O2	0.7859(2)	−0.1285(2)	0.1119(3)	7.5(1)
O3	0.7829(3)	0.1641(3)	0.0317(3)	9.0(1)
O4	0.8481(3)	−0.0262(3)	0.0545(3)	9.5(1)
C8	0.5676(5)	−0.1811(4)	0.1921(4)	7.6(2)
C9	0.4129(4)	0.1744(3)	0.0992(4)	7.0(2)
C10	0.7291(5)	−0.2624(4)	0.1980(4)	8.1(2)
C11	0.4675(5)	0.3055(4)	0.0336(5)	8.0(2)
O5	0.3506(3)	0.1594(3)	0.1256(3)	10.0(2)
O6	0.5027(4)	−0.1950(3)	0.2148(4)	11.6(2)
O7	0.4409(4)	0.3712(3)	0.0156(4)	11.3(2)
O8	0.7643(4)	−0.3246(3)	0.2245(4)	12.0(2)

$^a B_{eq} = \sum_i\sum_j U_{ij} a_i^* \cdot a_j^* \cdot \vec{a}_i \cdot \vec{a}_j$.

Anal. Calcd for $[NPr_4]_{0.5}[Ir_2(Dcbt)(CO)_4]$, $C_{14}H_{14}N_{3.5}O_8Ir_2$: C, 22.6; H, 1.90; N, 6.59. Found: C, 23.1; H, 1.92; N, 6.73. IR (KBr): 2099, 2076, 2046, 1995, 1970 cm^{-1} (CO), 1664 cm^{-1} (OCO asym).

X-ray Structure Determinations. Single crystals of $[NBu_4][Rh_2(Dcbt)(CO)_4]\cdot 0.4CH_2Cl_2$ were grown by layering hexane onto a solution of the product in methylene chloride. Two kinds of crystals were observed, green and red. The green ones lost solvent very easily and became red. The red crystals, which were also solvated, kept their crystallinity when sealed in a glass capillary. Only the red, less solvated crystals, were suitable for X-ray structure determination. Well-formed red crystals were sealed in a glass capillary and mounted on an Enraf-Nonius Model CAD4.

Single crystals of $[NBu_4][Rh_2(Dcbt)(CO)_2(PPh_3)_2]$ were grown by layering ether onto a solution of the product in acetonitrile. Well formed crystals were sealed in a glass capillary and mounted on a Syntex $P2_1$. Details of the X-ray data for the two crystal structures are reported in Table I. Unit cell dimensions and standard deviations were derived from 25 and 15 high-angle reflections for $[NBu_4][Rh_2(Dcbt)(CO)_4]\cdot 0.4CH_2Cl_2$ and $[NBu_4][Rh_2(Dcbt)(CO)_2(PPh_3)_2]$, respectively. Standard reflections remained constant during data collection, and data reduction was done by standard methods. The Patterson method and Fourier routines were used to solve the structures, which were refined by least-squares methods.[21] Hydrogen atoms were introduced in calculated positions, and the rest of the atoms were refined anisotropically, except the solvent atoms of the first structure and the carbons of the phenyl groups of the second structure. Tables II and III show the fractional atomic coordinates of the two structures.

Results and Discussion

Structure of $[NBu_4][Rh_2(Dcbt)(CO)_4]\cdot 0.4CH_2Cl_2$. A view of the complex anion is shown in Figure 1. Bond lengths and angles are summarized in Tables IV and V. The most characteristic feature of the anion is its planarity. The highest deviation from the mean plane defined by all the atoms of the anion is 0.35 Å. Only six atoms are separated more than 0.1 Å from this plane: O8 (−0.35 Å), O3 (−0.25 Å), C10 (−0.21 Å), O5 (−0.13 Å), O4 (0.13 Å), and C7 (−0.10 Å). The dihedral angle between the two mean planes containing one Rh and their four donor atoms is only 3.4°.

The geometry about each rhodium atom can be described as square planar. The major distortion from the ideal square-planar geometry is due to the bit angle of 79.3° of the chelating fragment O–Rh–N. This value is close to those observed for other complexes

(21) Sheldrick, G. M. SHELXS86. In *Crystallographic Computing 3*; Sheldrick, G. M.; Krüger, C., Goddard, R., Eds.; 1985. Sheldrick, G. M. SHELX76: Program for crystal structure determination. University of Cambridge, England, 1976.

Table III. Selected Fractional Atomic Coordinates for $[NBu_4][Rh_2(Dcbt)(CO)_2(PPh_3)_2]$

atom	x/z	y/b	z/c	B_{eq}, Å^2
Rh1	-0.02150(3)	0.20747(5)	0.33522(5)	2.96(2)
Rh2	0.32814(3)	0.23245(5)	0.33865(5)	3.20(2)
N1	0.0908(3)	0.2320(5)	0.3207(5)	3.1(2)
N2	0.1583(3)	0.2149(5)	0.3710(5)	3.3(2)
N3	0.2115(3)	0.2372(5)	0.3203(5)	3.0(2)
C4	0.1779(4)	0.2672(6)	0.2352(6)	3.1(3)
C5	0.1000(4)	0.2638(6)	0.2371(6)	2.8(2)
C6	0.2326(5)	0.2924(7)	0.1712(7)	3.9(3)
C7	0.0272(4)	0.2875(6)	0.1745(6)	3.4(3)
O1	-0.0346(3)	0.2669(5)	0.2074(4)	3.8(2)
O2	0.3024(3)	0.2738(5)	0.2016(4)	3.9(2)
O3	0.0279(3)	0.3235(5)	0.1004(5)	4.5(2)
O4	0.2126(3)	0.3306(6)	0.0997(5)	5.3(3)
C8	0.3425(5)	0.2107(8)	0.4665(8)	4.7(4)
C9	0.0023(4)	0.1594(7)	0.4488(7)	3.6(3)
O5	0.0217(4)	0.1305(6)	0.5204(5)	5.7(3)
O6	0.3484(4)	0.2017(8)	0.5492(7)	8.2(4)
P1	-0.1511(1)	0.1903(2)	0.3273(2)	2.97(3)
P2	0.4543(1)	0.2215(2)	0.3363(2)	3.53(7)

^{a} $B_{eq} = \sum_i \sum_j U_{ij} a_i^* \cdot a_j^* \cdot \vec{a}_i \vec{a}_j$.

Table IV. Selected Bond Distances (Å) for $[NBu_4][Rh_2(Dcbt)(CO)_4]$

Rh1-N1	2.037(4)	C4-C6	1.493(7)
Rh1-O1	2.056(5)	C6-O4	1.212(8)
Rh1-C9	1.811(7)	C6-O2	1.295(7)
Rh1-C11	1.858(6)	C5-C7	1.496(7)
Rh2-N3	2.029(4)	C7-O3	1.210(8)
Rh2-O2	2.036(4)	C7-O1	1.291(7)
Rh2-C8	1.838(8)	C8-O6	1.133(10)
Rh2-C10	1.848(6)	C10-O8	1.122(8)
N1-N2	1.313(5)	C9-O5	1.141(9)
N2-N3	1.327(5)	C11-O7	1.122(8)
N3-C4	1.350(7)	Rh1···Rh2′	3.336(1)
C4-C5	1.363(6)	Rh1···Rh2	6.135(1)
C5-N1	1.349(6)		

Table V. Selected Bond Angles (deg) for $[NBu_4][Rh_2(Dcbt)(CO)_4]$

C11-Rh1-O1	93.1(2)	N2-N1-Rh1	135.1(3)
O1-Rh1-N1	79.3(2)	C5-N1-Rh1	113.8(3)
C9-Rh1-N1	97.5(2)	C7-C5-N1	116.1(4)
C11-Rh1-C9	90.0(3)	C7-C5-C4	137.5(5)
O2-Rh2-N3	79.5(2)	C6-C4-C5	138.5(5)
C10-Rh2-O2	92.9(2)	C6-C4-N3	115.6(4)
C10-Rh2-C8	90.3(9)	C4-N3-Rh2	113.9(3)
C8-Rh2-N3	97.3(2)	N2-N3-Rh2	135.1(3)
O5-C9-Rh1	178.2(5)	O1-C7-O3	123.7(5)
O7-C11-Rh1	177.7(7)	O3-C7-C5	122.6(5)
O6-C8-Rh2	179.7(6)	O1-C7-C5	113.7(5)
O8-C10-Rh2	179.2(6)	O4-C6-C4	121.6(5)
N3-N2-N1	106.1(4)	O4-C6-O2	124.7(5)
C4-N3-N2	110.8(4)	O2-C6-C4	113.7(5)
C5-C4-N3	105.8(4)	C7-O1-Rh1	116.9(4)
C5-N1-N2	111.0(4)	C6-O2-Rh2	117.1(4)
C4-C5-N1	106.3(4)		

of dicarboxyazolate ligands such as 4,5-dicarboxyimidazolate,[6] 2-methyl-4,5-dicarboxyimidazolate,[8] and 3,5-dicarboxypyrazolate.[9] The distances from the metal to the donor atoms of the ligand are similar to those found in $[NBu_4][Rh_2(Dcbp)(CO)_4]$ (Dcbp = 3,5-dicarboxypyrazolate).[9] The distance between the two rhodiums of the molecule is 6.35 Å, which is about the same as that reported for the anion $[Rh_2(Dcbi)(cod)_2]^-$ (Dcbi = 3,5-dicarboxyimidazolate).[6] As expected, the distances in the aromatic ring indicate that the negative charge of the heterocycle is mainly shared by N1 and N3. A substantial negative charge supported by N2 would produce a longer C4-C5 bond and shorter C4-N3 and C5-N1 bonds, compared with those of coordinated dicarboxyimidazolates.[6,8]

An interesting feature of the structure is the packing of the ions in the crystal. It consists of dimeric units of anions separated by cations. The two anions in the dimer are related by an inversion

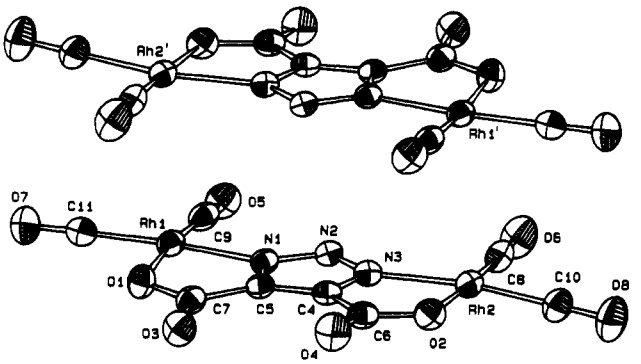

Figure 1. View of the dimeric unit of the complex anion in $[NBu_4][Rh_2(Dcbt)(CO)_4]$.

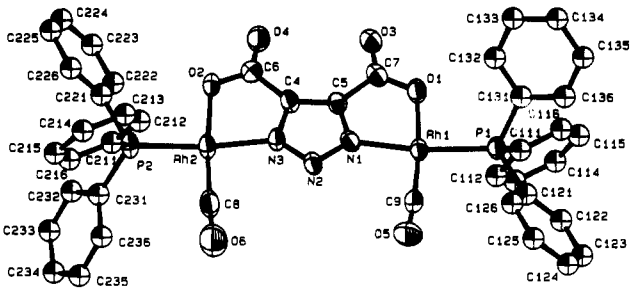

Figure 2. ORTEP diagram of the complex anion in $[NBu_4][Rh_2(Dcbt)(CO)_2(PPh_3)_2]$.

center and adopt an eclipsed configuration. Figure 1 illustrates that one anion is a little slipped from the other. The Rh2-Rh1-Rh2′ angle is 82.9°. The intermolecular rhodium-rhodium distance in the dimer is only 3.336 Å. These metal-metal interactions are responsible of the red color of the salt (the complex is yellow in solution).

Also worth noting, is the pseudoplanar conformation of the cations. In order to achieve a better packing, the tetrabutylammoniums mimic the planar geometry of the anions and adopt the flatest conformation compatible with the tetrahedral angles of carbon and nitrogen.

Structure of $[NBu_4][Rh_2(Dcbt)(CO)_2(PPh_3)_2]$. An ORTEP diagram of the anion $[Rh_2(Dcbt)(CO)_2(PPh_3)_2]^-$ is given in Figure 2. It shows that the PPh_3 ligands are situated *trans* to N. This result is consistent with other structure determinations of mononuclear complexes such as [Rh(oxine)(CO)(PPh_3)] (oxine = 8-hydroxyquinoline),[22] [Rh(SAL-NR)(CO)(PPh_3)] (SAL-NR = *N*-*o*-tolylsalicylaldiminate),[23] and [Rh(pic)(CO)(PPh_3)] (pic = 2-carboxypyridinate).[24] In the case of the present dinuclear complex, the *trans*-N disposition of the triphenylphosphine can be attributed both to the larger *trans* effect of the nitrogen and to steric demands, since the isomer with the phosphines *trans* to O would be subject to unfavorable interaction between the two phosphorus ligands. Bond distances and angles for this structure are listed in Tables VI and VII. Most of the distances from the rhodium to the donor atoms are similar those found in the mononuclear complex [Rh(pic)(CO)(PPh_3)]. By contrast, the Rh-N distances of 2.038 and 2.042 Å in the dinuclear complex are significantly shorter than the value of 2.088(6) Å reported for the mononuclear 2-carboxypyridinate complex. The difference can be attributed to the higher polarity of the Rh-N bond in the dinuclear complex, because of the negative charge of the azolate ring. The rhodium-carbonyl distances are slightly shorter in $[Rh_2(Dcbt)(CO)_2(PPh_3)_2]^-$ than in $[Rh_2(Dcbt)(CO)_4]^-$, corre-

(22) Leipoldt, J. G.; Basson, S. S.; Dennis, C. R. *Inorg. Chim. Acta* **1981**, *50*, 121.
(23) Leipoldt, J. G.; Basson, S. S.; Grobler, E. C.; Roodt, A. *Inorg. Chim. Acta* **1985**, *99*, 13.
(24) Leipoldt, J. G.; Basson, S. S.; Graham, D. E. *Inorg. Chim. Acta* **1985**, *101*, 123.

Table VI. Selected Bond Distances (Å) for $[NBu_4][Rh_2(Dcbt)(CO)_2(PPh_3)_2]$

Rh1–N1	2.039(6)	C4–C5	1.382(10)
Rh1–O1	2.070(7)	C5–N1	1.341(12)
Rh1–P1	2.262(2)	C4–C6	1.490(13)
Rh1–C9	1.811(10)	C6–O4	1.220(13)
Rh2–N3	2.041(5)	C6–O2	1.295(10)
Rh2–O2	2.051(6)	C5–C7	1.509(11)
Rh2–P2	2.261(2)	C7–O3	1.224(12)
Rh2–C8	1.796(12)	C7–O1	1.291(10)
N1–N2	1.328(8)	C8–O6	1.136(15)
N2–N3	1.324(9)	C9–O5	1.140(13)
N3–C4	1.364(11)	Rh1···Rh2	6.202(4)

Table VII. Selected Bond Angles (deg) for $[NBu_4][Rh_2(Dcbt)(CO)_2(PPh_3)_2]$

P1–Rh1–O1	91.9(2)	C5–N1–Rh1	115.2(5)
O1–Rh1–N1	78.5(3)	C7–C5–N1	115.3(7)
C9–Rh1–N1	94.8(3)	C7–C5–C4	137.9(7)
P1–Rh1–C9	94.8(3)	C6–C4–C5	139.9(8)
O2–Rh2–N3	78.3(3)	C6–C4–N3	114.6(7)
P2–Rh2–O2	95.4(2)	C4–N3–Rh2	115.1(5)
P2–Rh2–C8	90.8(3)	N2–N3–Rh2	134.7(5)
C8–Rh2–N3	95.8(4)	O1–C7–O3	124.2(7)
O5–C9–Rh1	176.1(8)	O3–C7–C5	122.4(7)
O6–C8–Rh2	175.5(9)	O1–C7–C5	113.5(7)
N3–N2–N1	107.1(6)	O4–C6–C4	121.8(8)
C4–N3–N2	110.2(6)	O4–C6–O2	124.4(9)
C5–C4–N3	105.4(7)	O2–C6–C4	113.8(7)
C5–N1–N2	110.4(6)	C7–O1–Rh1	117.3(5)
C4–C5–N1	106.8(6)	C6–O2–Rh2	117.8(5)
N2–N1–Rh1	134.1(5)		

Scheme I

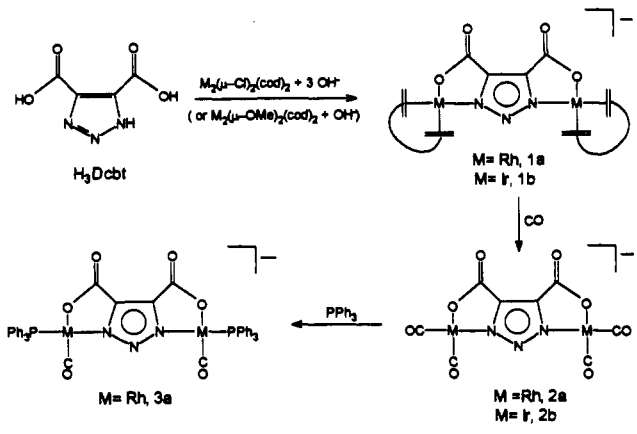

sponding to the higher π-acceptor character of the carbonyl compared with the phosphine. As in the tetracarbonyl structure, the ring distances in $[Rh_2(Dcbt)(CO)_2(PPh_3)_2]^-$ suggest that the ring negative charge is held mainly on N1 and N3. The geometry about the rhodium atom is approximately square planar (the sum of the bond angles around the metal is 360°). Again, the bite angle of 78° of the five member chelate ring is the largest deviation from the square-planar geometry. The calculation of the mean plane through the atoms of the $Dcbt^{3-}$ ligand showed it to be planar, within experimental error, and coplanar with the coordination metallic centers. The largest deviations from planarity of all the atoms of the anion (except the phenyl groups) are associated with O3 (0.17 Å), P1 (–0.14 Å), O5 (–0.14 Å), O2 (–0.19 Å), P2 (–0.33 Å), C8 (0.18 Å), and O6 (0.41 Å). The remaining atoms deviate less than 0.1 Å from this plane.

Rh(I) and Ir(I) Compounds. The chemical structures of the Rh(I) and Ir(I) compounds are shown in Scheme I. The properties and the chemistry of the dinuclear compounds with $Dcbt^{3-}$ as bridging ligand are analogous to those found for the products with other dicarboxyazolates.[6,8,9] 4,5-Triazoledicarboxylic acid (H_3Dcbt) reacts with $[M_2(\mu\text{-}Cl)_2(cod)_2]$ (M = Rh, Ir) and 3 equiv of $[NR_4]OH$ in acetonitrile to afford the yellow crystalline dinuclear salts $[NR_4][M_2(Dcbt)(cod)_2]$ (see **1a,b**). Alternatively, $[Ir_2(\mu\text{-}OMe)_2(cod)_2]$ may be used instead of $[Ir_2(\mu\text{-}Cl)_2(cod)_2]$. In this case, only 1 equiv of base is necessary and yields and purity of the products are better. In the solid state, the rhodium complexes are stable in air over long periods. However, the iridium compounds must be stored under nitrogen.

The IR spectra of these compounds are dominated by the strong asymmetric carboxylate bands which appear in the region 1610–1665 cm^{-1}, as expected for a monodentate carboxylate group.[25] In the solid state, the position of this band depends on the counterion of the complex ion. This may be related to variable polarization of the carboxylate groups caused by the different cations.

The ^1H and ^{13}C NMR signals of cyclooctadiene for $[M_2(Dcbt)(cod)_2]^-$ appear in positions similar to those for other related compounds.[6,9] The *trans*-N and *trans*-O olefins of the cyclooctadiene appear as two distinct signals when $CDCl_3$ is used as solvent. However, in a stronger donor solvent like CD_3OD a rapid exchange takes place, yielding only one signal.

Slow bubbling of carbon monoxide through CH_2Cl_2 or CH_3CN solutions of the diolefin complexes affords the expected *cis*-dicarbonyl compounds $[NR_4][M_2(Dcbt)(CO)_4]$ (see **2a,b**). All of them crystallize as very dark dichroic needles with a metallic appearance. These features suggest strong anisotropy of the structure and the presence of extended intermolecular metal–metal interactions favored by the planarity of the dinuclear anions $[M_2(Dcbt)(CO)_4]^-$.

The IR spectra of $[M_2(Dcbt)(CO)_4]^-$ in CH_2Cl_2 solution show two equal-intensity bands characteristic of *cis*-dicarbonyl compounds of rhodium and iridium. However, when the spectra are recorded in the solid state, the carbonyl region shows a more complex pattern. This phenomenon has been observed in other planar $[M_2(A)(CO)_4]^-$ complexes (M = Rh, Ir; A = 4,5-dicarboxyimidazolate, 2-methyl-4,5-dicarboxyimidazolate, 3,5-dicarboxypyrazolate)[6,9] and in other cases of *cis*-dicarbonyl compounds of Rh(I) and Ir(I),[26] and it is usually attributed to carbonyl couplings through metal–metal interactions.

The complex anions $[Rh_2(Dcbt)(CO)_4]^-$ react with 1 equiv of PPh_3, giving the yellow crystalline products $[NR_4][Rh_2(Dcbt)(CO)_2(PPh_3)_2]$ (see **3a**). The resolution of the structure of $[NBu_4][Rh_2(Dcbt)(CO)_2(PPh_3)_2]$ revealed that the PPh_3 displaced only the *trans*-N carbonyl.

Oxidation Product of $[Rh_2(Dcbt)(CO)_4]^-$ and $[TTF][Rh_2(Dcbt)(CO)_4]\cdot 0.5CH_3CN\cdot H_2O$. When $[NBu_4][Rh_2(Dcbt)(CO)_4]$ was electrolyzed in acetonitrile, a dark dichroic product of composition $[Rh_2(Dcbt)(CO)_4]$ formed on the anode surface before the passivation of the electrode. The neutral complexes $[Rh_2(Dcbt)(CO)_4]$ can also be synthesized by chemical oxidation of $[Rh_2(Dcbt)(CO)_4]^-$ with oxidizing agents such as $[NO][BF_4]$ or $[C_7H_7][BF_4]$. In contrast to what we observed for other dinuclear rhodium anions,[7,9] when $[p\text{-}CH_3C_6H_4N_2][BF_4]$ was used as oxidant, the product obtained was not the expected one but $[p\text{-}CH_3C_6H_4N_2][Rh_2(Dcbt)(CO)_4]$, probably due to the insolubility of this salt.

$[Rh_2(Dcbt)(CO)_4]$, a formally Rh(I)–Rh(II) mixed-valence compound, is diamagnetic, like the others species $[Rh_2(A)(CO)_4]$ (A = 4,5-dicarboxyimidazolate, 2-methyl-4,5-dicarboxyimid-azolate) we previously reported.[7,9] Since Rh(II) is a d^7 ion, the diamagnetism of this compound suggests a structure with two units of $[Rh_2(Dcbt)(CO)_4]$ linked by a Rh(II)–Rh(II) bond.

When a solution of $[Rh_2(Dcbt)(CO)_4]^-$ and tetrathiafulvalene (TTF) was electrochemically oxidized, a dichroic product of composition $[TTF][Rh_2(Dcbt)(CO)_4]\cdot 0.5CH_3CN\cdot H_2O$ was obtained. This salt of TTF^+ and the dinuclear Rh(I) complex can also be prepared by metathesis of $[NBu_4][Rh_2(Dcbt)(CO)_4]$ and $[TTF]_3[BF_4]_2$. The infrared spectrum of $[TTF][Rh_2(Dcbt)(CO)_4]\cdot 0.5CH_3CN\cdot H_2O$ is dominated by a plasma

(25) Robinson, S. D.; Utley, M. F. *J. Chem. Soc., Dalton Trans.* **1973**, 1914.
(26) Bonati, F. *Organomet. Chem. Rev.* **1961**, *1*, 379.

edge characteristic of conductive materials. Its conductivity measured on a pressed pellet was $7 \times 10^{-5}\ \Omega^{-1}\ cm^{-1}$, and it is in the range of that found for other salts of dicarboxyazolates of the type $[TTF][Rh_2(A)(CO)_4]$. The value is typical of compounds [TTF][C], C being an inorganic anion, where the conductivity is due to interactions between the orbitals of the stacked TTF molecules and not to an electronic transfer between TTF and the anion.[27] In fact, the IR carbonyl bands of the anion $[Rh_2(Dcbt)(CO)_4]^-$ do not shift significantly when NBu_4^+ is substituted by TTF^+, supporting the idea that there is no charge transfer between anions and cations.

Oxidized Products $[NR_4]_{0.5}[Ir_2(Dcbt)(CO)_4]$ (R = Pr, Bu). Because of the low solubility of the salts of $[Ir_2(Dcbt)(CO)_4]^-$ with small cations (Na^+, K^+, NMe_4^+, NEt_4^+), only salts with larger cations could be used for electrochemical experiments. When $[NR_4][Ir_2(Dcbt)(CO)_4]$ (R = Pr, Bu) were electrolyzed in acetonitrile or CH_2Cl_2, dark materials grew on the anode surface. Since the current did not drop during the deposition, it may be inferred that these oxidation products are conductive materials. The solids obtained analyzed as $[NR_4]_{0.5}[Ir_2(Dcbt)(CO)_4]$. The formulation of these materials is the same as that found when similar iridium dicarboxyimidazolate and dicarboxypyrazolate complexes were oxidized.[7,9] In attempts to obtain X-ray-quality crystals of these compounds, solvent, temperature, and current density were varied. So far, all the attempts have been unsuccessful. These partially oxidized materials show a broad absorption edge in their infrared spectra. Their conductivities measured on pressed pellets are $8 \times 10^{-5}\ \Omega^{-1}\ cm^{-1}$ for $[NPr_4]_{0.5}[Ir_2(Dcbt)(CO)_4]$ and $2 \times 10^{-5}\ \Omega^{-1}\ cm^{-1}$ for $[NBu_4]_{0.5}[Ir_2(Dcbt)(CO)_4]\cdot 0.5CH_3CN$. These values are more than 100 times higher than those found for the unoxidized precursors. The higher value for the smaller cation is consistent with the idea that smaller cations allow better packing and therefore larger metal–metal interactions. These conductivities are nearly equal to those found for other dicarboxyazolate complexes, suggesting the same conduction mechanism for all of these compounds. In the case of highly anisotropic materials, the value of the conductivity measured on pressed pellets is often related to the value of the conductivity measured in the main-axis direction of the crystal by a factor of 10^3 approximately.[28] Therefore, it can be concluded that the conductivities of the partially oxidized salts $[NR_4]_{0.5}[Ir_2(A)(CO)_4]$ are in the same range of those found for the partially oxidized bis(oxalato)-platinates with large cations.[2] Furthermore, the presence of solvent in the composition of the partially oxidized salts and their tendency to lose it suggest that the conductivities might be higher for freshly prepared products.[2]

The XPS results obtained for the core levels of Ir and N in $[NPr_4][Ir_2(Dcbt)(CO)_4]$ and $[NBu_4]_{0.5}[Ir_2(Dcbt)(CO)_4]\cdot 0.5CH_3CN$ are displayed in Figures 3 and 4 and summarized in Table VIII. The Doniach–Sunjic formula was used for the deconvolution of the data.[29] Splitting of the $4f^{7/2}$ and $4f^{5/2}$ peaks of the iridium in $[NBu_4]_{0.5}[Ir_2(Dcbt)(CO)_4]\cdot 0.5CH_3CN$ occurred when the width of the peak was forced to be the same for both the oxidized and the unoxidized products. This phenomenon was also observed for $[NBu_4]_{0.5}[Ir_2(Dcbp)(CO)_4]$ (Dcbp = 3,5-dicarboxypyrazo-late)[9] and can be explained by the presence of two slightly different types of iridium at the same concentration in the structure of the partially oxidized product. Since the binding energies of the two signals of $[NBu_4]_{0.5}[Ir_2(Dcbt)(CO)_4]\cdot 0.5CH_3CN$ are higher than those of $[NBu_4][Ir_2(Dcbt)(CO)_4]$, it can be concluded that both types of iridium atoms are oxidized. The separation between the signals corresponding to the two iridium atoms is higher for $[NBu_4]_{0.5}[Ir_2(Dcbp)(CO)_4]$ (0.8 eV) (Dcbp = 3,5-dicarboxypyrazolate)[9] than for $[NBu_4]_{0.5}[Ir_2(Dcbt)(CO)_4]\cdot 0.5CH_3CN$ (0.4 eV). Only a single type of iridium signal is observed for $[NBu_4]_{0.5}[Ir_2(MDcbi)(CO)_4]\cdot 0.5CH_3CN$[7] or $[NPr_4]_{0.5}[Ir_2(Dcbp)(CO)_4]$[9] (MDcbi = 2-methyl-4,5-dicarboxyimidazolate; Dcbp = 3,5-dicarboxypyrazolate). The differences in the XPS suggest more than one type of structure for this family of partially oxidized materials. It seems that small cations and strictly flat anions favor more symmetrical structures (i.e. only one Ir signal occurs). It is interesting to note, that in all cases, the shift of the binding energy for the mixed-valence materials indicates that the oxidation is centered on the metal. This parallels the shift of the CO vibrations to higher energy observed for the oxidized products.

In either the oxidized or unoxidized compounds, the spectra

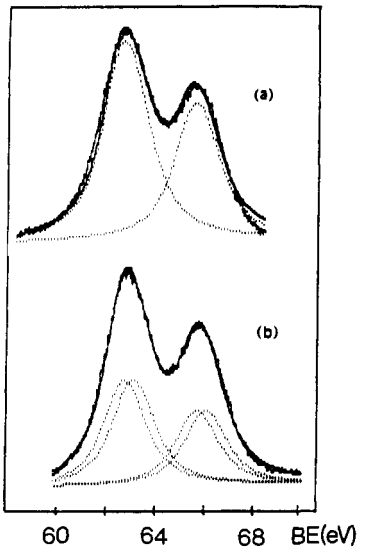

Figure 3. X-ray photoelectron spectra (XPS) in the iridium energy region: (a) $[NBu_4][Ir_2(Dcbt)(CO)_4]$; (b) $[NBu_4]_{0.5}[Ir(Dcbt)(CO)_4]\cdot 0.5CH_3CN$.

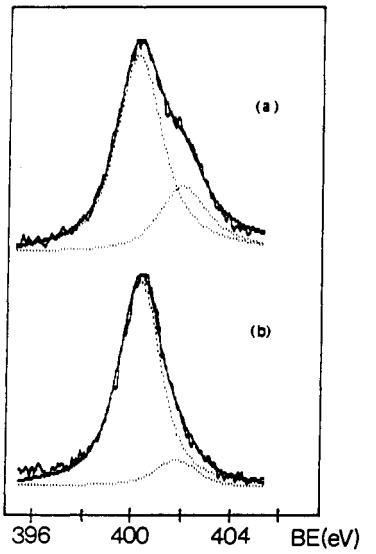

Figure 4. X-ray photoelectron spectra (XPS) in the nitrogen energy region: (a) $[NBu_4][Ir_2(Dcbt)(CO)_4]$; (b) $[NBu_4]_{0.5}[Ir_2(Dcbt)(CO)_4]\cdot 0.5CH_3CN$.

Table VIII. XPS Binding Energies in the Iridium and Nitrogen Regions for $[NBu_4]_x[IR_2(Dcbt)(CO)_4]$

	binding energy, eV	rel intens		binding energy, eV	rel intens
		$[NBu_4][Ir_2(Dcbt)(CO)_4]$			
$Ir[4f^{5/2}]$	62.35	1.0	$N[1s]_{ring}$	400.40	1.0
$Ir[4f^{7/2}]$	65.25	0.7	$N[1s]_{cation}$	402.15	0.3
		$[NBu_4]_{0.5}[Ir_2(Dcbt)(CO)_4]\cdot 0.5CH_3CN$			
$Ir[4f^{5/2}]$	63.12, 63.50	1.0	$N[1s]_{ring}$	400.65	0.6
$Ir[4f^{7/2}]$	66.25, 66.63	0.7	$N[1s]_{cation}$	402.15	0.1

(27) *Extended Linear Chain Compounds*; Miller, J. S., Ed.; Plenum: New York, 1983; Vol. 3, p 462.
(28) Coleman, L. B. *Rev. Sci. Instrum.* **1978**, *49*, 58.
(29) Doniach, S.; Sunjic, M. *J. Phys. Chem.* **1970**, *3*, 285.

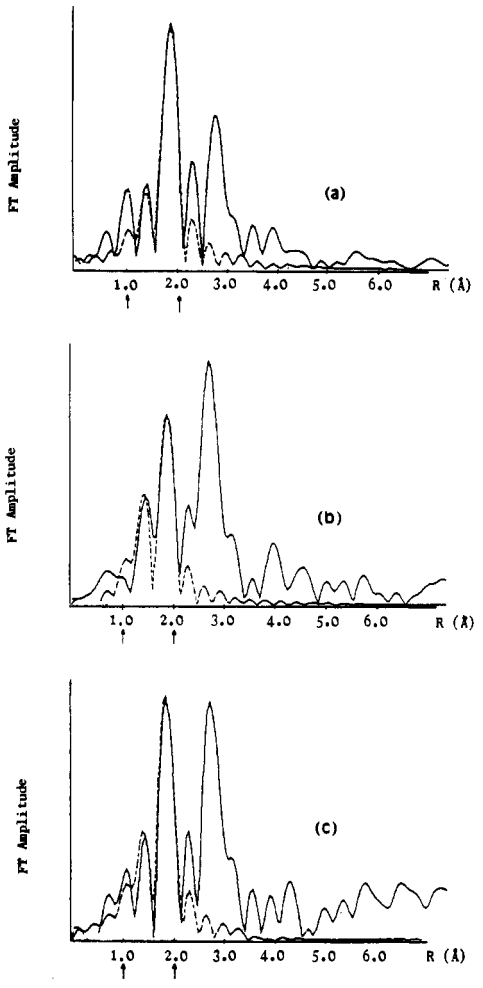

Figure 5. Moduli of the Fourier transforms of k^3-weighted EXAFS spectra (solid line): (a) $[NMe_4][Ir_2(Dcbt)(CO)_4]$; (b) $[NBu_4][Ir_2(Dcbt)(CO)_4]$; (c) $[NBu_4]_{0.5}[Ir_2(Dcbt)(CO)_4]\cdot 0.5CH_3CN$. The dashed lines correspond to the Fourier transforms calculated using the iridium first-coordination-shell parameters of Table IX.

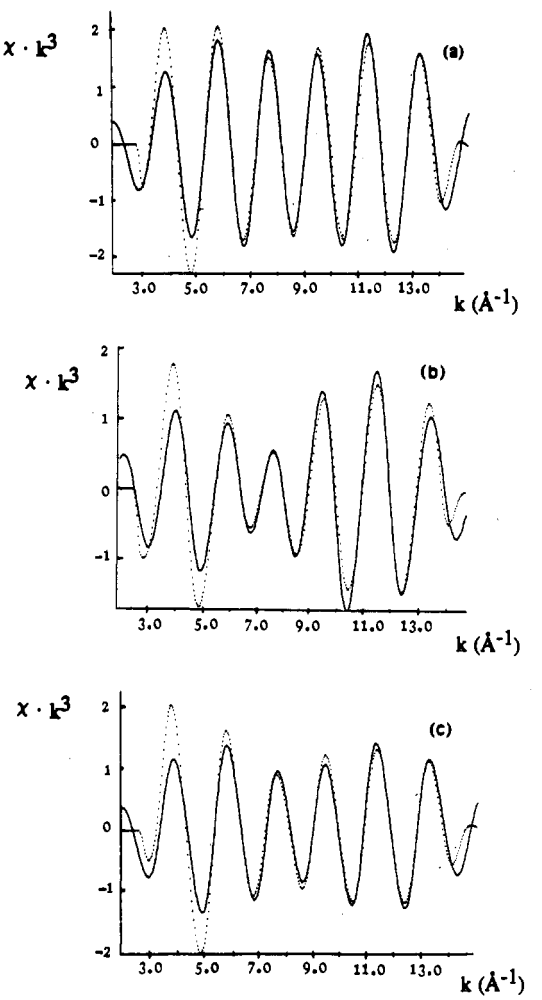

Figure 6. Back-Fourier transforms (filtered spectra) of the iridium first-coordination-shell EXAFS spectra (solid line): (a) $[NMe_4][Ir_2(Dcbt)(CO)_4]$; (b) $[NBu_4][Ir_2(Dcbt)(CO)_4]$; (c) $[NBu_4]_{0.5}[Ir_2(Dcbt)(CO)_4]\cdot 0.5CH_3CN$. The dotted lines are the calculated filtered EXAFS spectra of the iridium first coordination shell corresponding to the parameters of Table IX.

of N in the 1s region appear as two bands. The signal at lower energy corresponds to the N of the azolate ring while the otherhas to be assigned to the N of the cation. As we found previously,[7,9] the measure of the relative intensities of the two bands provides an unambiguous method to calculate the stoichiometry and therefore the degree of partial oxidation of the oxidized materials. The validity of this method has been corroborated with the species reported here. In this case, the ratios are 3:1 for the Ir(I) complex salt and 3:0.5 for the oxidized material in agreement with the stoichiometry of these species.

In order to obtain structural information about the complex anion and its packing in the solid, we have recorded the EXAFS spectra of the Ir L_{III} absorption of $[NMe_4][Ir_2(Dcbt)(CO)_4]\cdot 3H_2O$, $[NBu_4][Ir_2(Dcbt)(CO)_4]$, and $[NBu_4]_{0.5}[Ir_2(Dcbt)(CO)_4]\cdot 0.5CH_3CN$. Figure 5 shows the radial distribution obtained through the Fourier transform of the EXAFS spectra of these compounds. The study of the first coordination shell of the iridium was carried out analyzing the region between 1 and 2.2 Å of the radial distribution. Figure 6 shows the EXAFS spectra due to the atoms situated between 1 and 2.2 Å from the absorbent (back-Fourier transform of this zone in Figure 5). The best curve-fitting analysis obtained in this region is represented by dotted lines in Figures 5 and 6, and it corresponds to the structural models described in Table IX. Because of the good fitting of the models, it can be concluded that in the oxidized material the metal atom is linked to one O, one N, and two C atoms, at bond distances similar to those of the closely related rhodium tetracarbonyl structure discussed above. In order to reduce the number of parameters during the curve fitting, only a Ir–C distance was used. Since

Table IX. EXAFS Curve-Fitting Results for the Compounds $[R_4N]_x[Ir_2(Dcbt)(CO)_4]$

	C[a]	O[a]	N[a]	Ir[b]	O(CO)[b]	C(N)[b,c]
			$[NMe_4][Ir_2(Dcbt)(CO)_4]$			
N[e]	2	1	1	2	2	2
R_f[f] Å	1.92	2.07	2.09	2.87	3.05	2.88
$10^3\sigma^2$,[g] Å^2	10	2.5	2.5	3.1[d]	0.9	10
ΔE_0,[h] eV	15	15	15	14.1	14.1	15.2
			$[NBu_4][Ir_2(Dcbt)(CO)_4]$			
N	2	1	1	1.5	2.7	2.3
R, Å	1.88	2.07	2.06	2.88	2.96	2.87
$10^3\sigma^2$, Å^2	6.2	3.5	3.5	5.1[d]	4.5	5.2
E_0, eV	14	14	14	10	14	14
			$[NBu_4]_{0.5}[Ir_2(Dcbt)(CO)_4]\cdot 0.5CH_3CN$			
N	2	1	1	2	2	2
R, Å	1.92	2.08	2.09	2.88	3.04	2.86
$10^3\sigma^2$, Å^2	8.5	3.0	3.0	4.3[d]	1.2	7.9
ΔE_0, eV	16	16	16	14.5	14	14

[a] Atoms in the first coordination sphere of iridium. [b] Atoms in the second shell of iridium. [c] Light atoms other than O of the carbonyl (see text). [d] Referred to Ir metal. [e] Number of atoms. [f] Averaged distance. [g] Debye–Waller factor. [h] Threshold dephase.

slightly different distances have been found for the *trans*-N and *trans*-O carbonyls in the X-ray-solved structures of these type compounds, a higher Debye–Waller factor was obtained for the C atoms when compared with the rest of atoms of the first

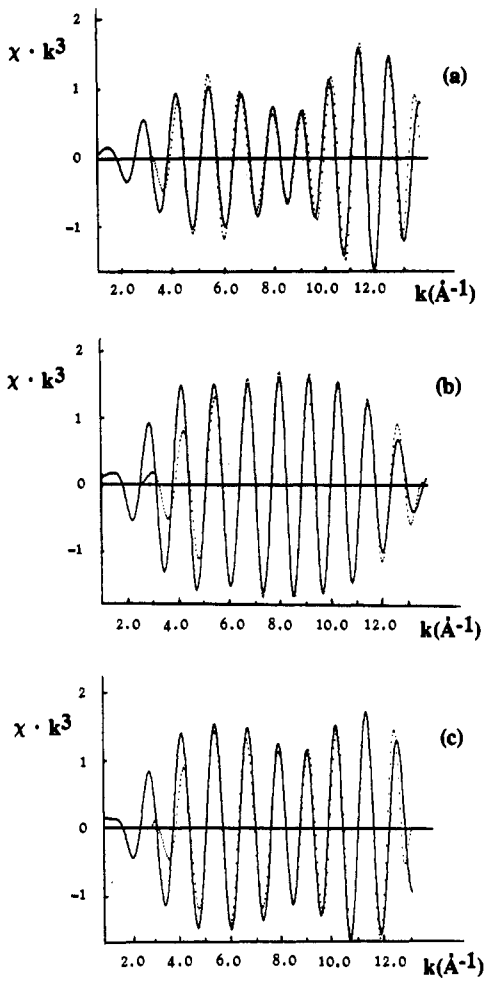

Figure 7. Back-Fourier transforms (filtered spectra) of the iridium second-shell EXAFS spectra (solid line): (a) $[NMe_4][Ir_2(Dcbt)(CO)_4]$; (b) $[NBu_4][Ir_2(Dcbt)(CO)_4]$; (c) $[NBu_4]_{0.5}[Ir_2(Dcbt)(CO)_4]\cdot 0.5CH_3CN$. The dotted lines are the calculated filtered EXAFS spectra of the iridium second shell corresponding to the parameters of Table IX.

coordination sphere. The important conclusion of these results is that, upon oxidation, the coordination sphere of the iridium is preserved.

As can be observed in the Fourier transforms of Figure 5, the radial distributions of three compounds show a strong peaks around 3 Å. According to the distances found in X-ray structure of the homologous rhodium complex, the associated oscillations must be attributed to two O atoms of the carbonyl groups, the C atoms of the carboxylic group and the triazole, the noncoordinated N of the ring, and the intermolecular Ir–Ir vector. Owing to the well-known focusing effect of C in the collinear Ir–C–O system,[30] the amplitude of the oscillations associated with the Ir–O(CO) pairs is expected to be greatly enhanced with respect to the other Ir–light atom systems. Therefore, the despite of the apparent complexity of the system, the EXAFS corresponding to the second shell should be dominated by the Ir–Ir and the Ir–O(CO) contributions. Figure 7 shows the back-Fourier transforms for the region between 2.5 and 3 Å in the radial distributions of Figure 5 (it corresponds to the contribution to the EXAFS of the peaks between these two distances). The filtered spectra in Figure 7a,c show in k space two distinct regions characterized by different phases and separated by a beat. It is known that oscillations due to Ir–Ir contributions show relatively small amplitudes in the low-k region and large ones in the high-k region. This pattern is greatly magnified when the spectrum is k^3 weighted. Therefore, the oscillations in the low-k region could be mainly associated with Ir–O(CO) pairs, while oscillations at k above 9 are essentially influenced by the Ir–Ir vectors. On the basis of that approach, the following strategy was used for the three spectra to obtain structural information about the second coordination shell of the iridium. First, independent fittings of the filtered EXAFS spectra were carried out, in both the low-k and the high-k region by modifying the parameters of the Ir–O(CO)[31] and Ir–Ir vectors, respectively. Then, the spectra were fitted in the entire k space by a two-atom shell model, using the best parameters found in the first step as starting values. Finally, the contributions of the rest of the second-shell light scatters were introduced, and the complete model was fitted by a series of least-squares cycles. Since it is known that the last light atoms have a small contribution to the spectra, they were treated as C atoms with a single Ir–C distance. In that way, the number of adjustable parameters was kept low enough to consider the calculation reliable. The structural parameters obtained for the second coordination shell are also shown in Table IX.

As expected, and because of the approximations used, the accuracy in the distances from the Ir to the light atoms were not too good for EXAFS. However, the Ir–Ir distance was found to be highly stable with respect to the set of parameters used for the light scatters. It is somewhat surprising that the same values were found for the Ir–Ir distances in the Ir(I) species and in the partially oxidized material. In other anisotropic conductors, a shortening in the metal–metal distance has been found upon partial oxidation. However, a recent report on Ir–Ir distances in anisotropic materials, carried out by EXAFS, showed Ir–Ir intermolecular distances in the range 2.8–2.9 Å in Ir(I) complexes,[32] which gives support to our results. On the other hand, the usual strong correlation between the number of scatterers and the Debye–Waller factor lends a degree of uncertainty to the number of Ir–Ir close contact. As a matter of fact, the number of iridium atoms in the second coordination sphere changes from 1 to 2, when σ^2 (measured with respect to the Ir metal) changes from 0 to 0.0035. Although a definitive conclusion cannot be extracted from these data, a model with more than one close Ir–Ir contact seems more reasonable, since the thermal motion should be smaller for metallic iridium than for these complex salts. In summary, the results of the analysis of the second shell are less conclusive than the ones of the first shell, but two aspects are notable. First, Ir–Ir intermolecular distances are quite similar for the Ir(I) species and the partially oxidized material, and they seem to be quite independent of the method used to extract the information from the spectra. Second, the packing of $[NBu_4]_{0.5}[Ir_2(Dcbt)(CO)_4]$ resembles that of the nonoxidized compound $[NMe_4][Ir_2(Dcbt)(CO)_4]$ and appears different from that of $[NBu_4][Ir_2(Dcbt)(CO)_4]$. It seems that in the oxidized material, the loss of half of the bulky NBu_4^+ cations allows a more compact structure, similar to that of the unoxidized salt with the small, NMe_4^+ cation.

Conclusions

Although $Dcbt^{3-}$ has an extra potentially coordinating N atom, the two X-ray-solved structures indicate that it behaves like the 4,5-dicarboxyimidazolate type ligands in terms of its coordination geometry. The study of this ligand has revealed several interesting new features, however.

The structure determination of $[NBu_4][Rh_2(Dcbt)(CO)_2(PPh_3)_2]$ corroborated the hypothesis we had made previously of the *trans*-N disposition of PPh_3, on both steric and electronic

(30) Teo, B. K. *J. Am. Chem. Soc.* **1981**, *103*, 3990.

(31) Because of the focusing effect, a phase shift equal to π was required for the Ir–O(CO) pairs, in order to achieve reasonable distances. This approach worked better than a ΔE_0 shift. The focusing effect is also responsible for the low σ^2 values obtained when the number of O(CO) scatters was kept low.

(32) Carr, N.; Crossley, J. G.; Dent, A. J.; Gouge, J. R.; Greaves, G. N.; Jarret, P. S.; Orpen, A. G. *J. Chem. Soc., Chem. Commun.* **1990**, 1369.

grounds, for the other $[Rh_2(A)(CO)_2(PPh_3)_2]^-$ compounds (A = 4,5-carboxyimidazolates,[6] 3,5-dicarboxypyrazolate[9]).

All the dinucleating dicarboxyazolate ligands can form conductive materials with the composition $[NR_4]_{0.5}[Ir_2(A)(CO)_4]$ (R = Pr, Bu; A = 4,5-dicarboxyimidazolate, 2-methyl-4,5-dicarboxyimidazolate, 3,5-dicarboxytriazolate, 3,5-dicarboxypyrazolate). The structure of the anion does not change during oxidation. The charge balance in the oxidized product is achieved only by loss of the cation. The presence of fewer cations in the oxidized products allows a better packing and therefore can accommodate the increased intermolecular metal–metal interactions.

The fact that only iridium formed partially oxidized conductors corroborates the idea that only the third-row transition metals have their d_{z^2} orbitals sufficiently diffused to overlap well at or near 3 Å (the minimum approximation distance of the orbitals of the ligands). Oxidation of the rhodium systems is accompanied by metal–metal bond formation but only in one direction.

Our work has shown that the formation of partially oxidized conductive complexes is a fairly general phenomenon in iridium compounds, providing that the ligands are carefully selected. Several stacking motifs which have been proposed for dinuclear species have been observed.[33] It is possible that the increased understanding of these stacking motifs will allow improved control over properties, especially in combination with other work regarding Coulombic effects on mixed-valence stacking.[34]

Acknowledgment. J.C.B. acknowledges DGICYT (Project PB88-0252) for financial support, and P.G.R. acknowledges support from the donors of the Petroleum Research Fund, administered by the American Chemical Society. We thank William Butler for the X-ray data collection of the second structure, LURE (Paris) for allowing us to use its synchrotron facilities, and R. Touroude from the Laboratoire de Catalyse et Chimie des Surfaces (Strasbourg, France) for allowing us to perform the XPS experiments.

Supplementary Material Available: Tables giving crystal data and details of the structure determinations, atom coordinates, and bond distances and angles for the two structures reported (21 pages). Ordering information is given on any current masthead page.

(33) Mueller-Westerhoff, U. Y.; Heinrich, F. In *Extended Interactions between Metal Ions*; Interrante, L. V., Ed.; ACS Symposium Series 5; American Chemical Society: Washington, DC, 1974; Chapter 28, pp 392–401.

(34) Ward, M. D.; Johnson, D. C. *Inorg. Chem.* **1987**, *26*, 4213.